Supplementary information for

A Novel Hybrid Carbon Material

Albert G. Nasibulin, Peter V. Pikhitsa, Hua Jiang, David P. Brown, Arkady V. Krasheninnikov, Anton S. Anisimov, Paula Queipo, Anna Moisala, David Gonzalez, Gunther Lientschnig, Abdou Hassanien, Sergey D. Shandakov, Giulio Lolli, Daniel E. Resasco, Mansoo Choi, David Tománek, and Esko I. Kauppinen*

*To whom correspondence should be addressed.

E-mail: esko.kauppinen@hut.fi, albert.nasibulin@hut.fi

Description of the experimental setups

In the ferrocene experimental reactor, catalyst particles were grown *in situ* via ferrocene vapour decomposition[1,2] (Figure S1a). The precursor was vaporized by passing ambient temperature CO (with a flow rate of 300 cm^3/min) through a cartridge filled with ferrocene powder. The partial vapour pressure of ferrocene in the reactor was maintained at 0.7 Pa. The flow containing ferrocene vapour was then introduced into the high temperature zone of the ceramic tube reactor through a water-cooled probe and mixed with additional CO (100 cm^3/min). The reactor wall temperature was varied from 800 to 1150 °C. Typically, single-walled carbon nanotubes (SWNTs) produced by this method were approximately 1.3 nm in diameter[2].

The HWG method for the production of SWNTs has been described elsewhere[3]. Briefly, this method relies on the introduction of preformed catalyst particles into a carbon nanotube synthesis reactor (Figure S1b). The particles were produced by vaporization from a resistively heated iron wire and subsequent cooling in a hydrogen containing flow at 400 cm^3/min. Particles were consequently formed and grown by vapour nucleation, condensation and coagulation processes. Subsequently, the produced particles were introduced into a ceramic tubular reactor, mixed with a carbon monoxide flow (400 cm^3/min) and heated (from 600 to 1200 °C) to induce SWNT formation. This method allows us to produce SWNTs with diameters in the range from 1.2 to 1.4 nm [4].

In both reactors, for the synthesis of NanoBuds, a controlled amount of water and carbon dioxide was added together with the carbon source. For this purpose, a mass flow controller (MFC) was used to introduce the carbon dioxide and/or water. In order to introduce the water vapour, a flow of a carrier gas was passed through a water saturation vessel. The amount of introduced water vapour was varied from 0 to 405 ppm. The concentration of introduced CO_2 was varied from 0 to 5000 ppm in the HWG case and from 0 to 12000 ppm in the ferrocene case. The carrier gas water vapour saturation conditions were monitored on-line by a Gasmet Fourier-transform infrared (FT-IR) spectrometer.

NanoBuds were collected downstream of the reactor either by filtering on silver or nitrocellulose disk filters or by depositing on TEM grids via an electrostatic precipitator (ESP). The morphology and

crystallinity of the as-obtained product were investigated with a field emission transmission electron microscope (Philips CM200 FEG).

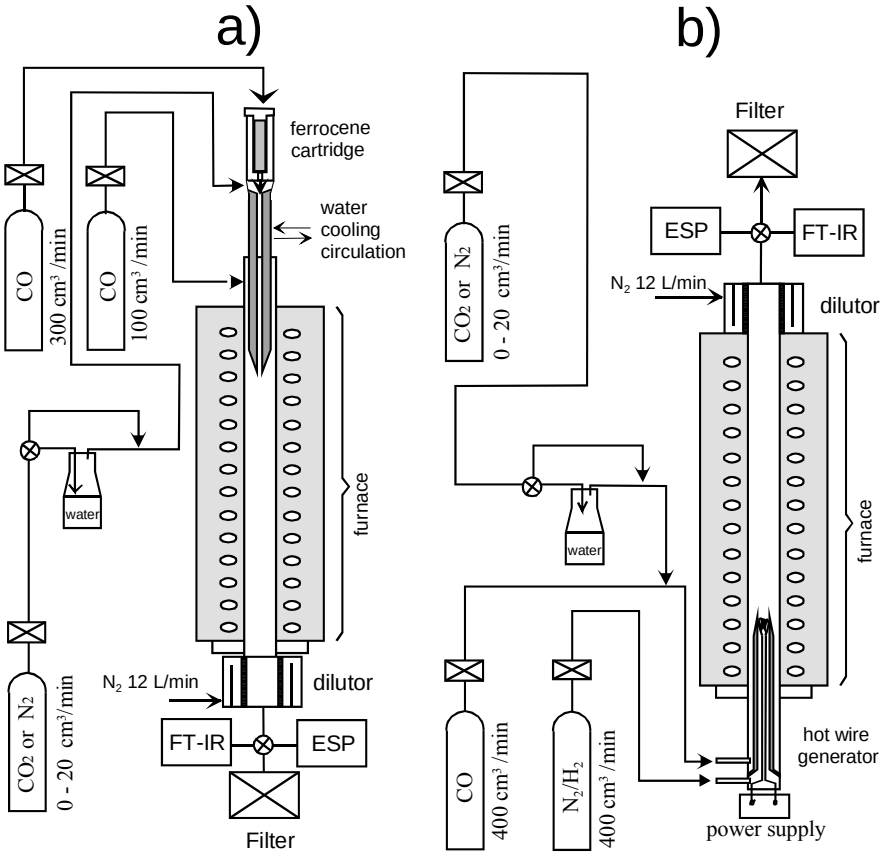

Figure S1. Schematics of the experimental setups: (a) ferrocene reactor, (b) HWG method.

It is worth noting that, even without intentionally introducing water and carbon dioxide, some H_2O and CO_2 were formed in the reactor[5]. Since catalyst material is always deposited, to some extent, on the reactor walls, CO disproportionation:

$$CO_{(g)}+CO_{(g)} \Leftrightarrow C_{(s)}+CO_{2(g)}, \Delta H = -169 \text{ kJ/mol} \quad (1)$$

and CO hydrogenation[6]:

$$H_{2(g)}+CO_{(g)} \Leftrightarrow C_{(s)}+ H_2O_{(g)}, \Delta H = -136 \text{ kJ/mol} \quad (2)$$

reactions can occur. FT-IR measurements[5] of the gaseous composition after the reactor revealed the presence of CO_2 with concentrations of 120 and 1540 ppm in the HWG and ferrocene reactor, respectively. The concentrations of water vapour were consistently below 10 ppm.

Control of the level of fullerene functionalisation of SWNTs

In an attempt to control the level of SWNT fullerene functionalisation, we have carried out systematic investigations of the effect of the reactor temperature and of the concentrations of water vapour and carbon dioxide. We found that these parameters noticeably affect the density of fullerenes on the surface of the tubes.

The separate and mutual introduction of H_2O and CO_2 in the ferrocene reactor revealed that the optimal reagent concentrations were between 45 and 245 ppm for H_2O and between 2000 and 6000 ppm for CO_2 with the highest fullerene density on individual SWNTs above 1 fullerene/nm. The preferred conditions for NanoBud formation were found when the H_2O concentration was between 125 and 185 ppm and the CO_2 concentration was approximately 2500 ppm.

An example of the change of the product morphology with the reactor conditions is shown in Figure S2, wherein the effect of water vapour concentration in the reactor at a reactor temperature of 1000 °C is clearly seen. Experimental conditions without adding water resulted in the formation of largely pure SWNTs together with non-active catalyst particles. NanoBuds start to form in abundance at a water vapour concentration of 45 ppm and higher. Conversely, at high concentrations of H_2O (>365 ppm), the product contained a high fraction of inactive catalyst particles and few NanoBuds.

It was found that, at specific concentrations of reagents, the reactor temperature had an optimal range for the synthesis of NanoBuds with high fullerene densities. The effect of the reactor temperature on the product was studied with 145 ppm water vapour introduced in the reactor. At temperatures of 1100 and 1150 °C only non-active catalyst particles were observed. The maximum fullerene coverage was found at 1000 °C and the amount of bonded fullerenes on the surface of SWNTs rapidly decreased with decreasing temperature.

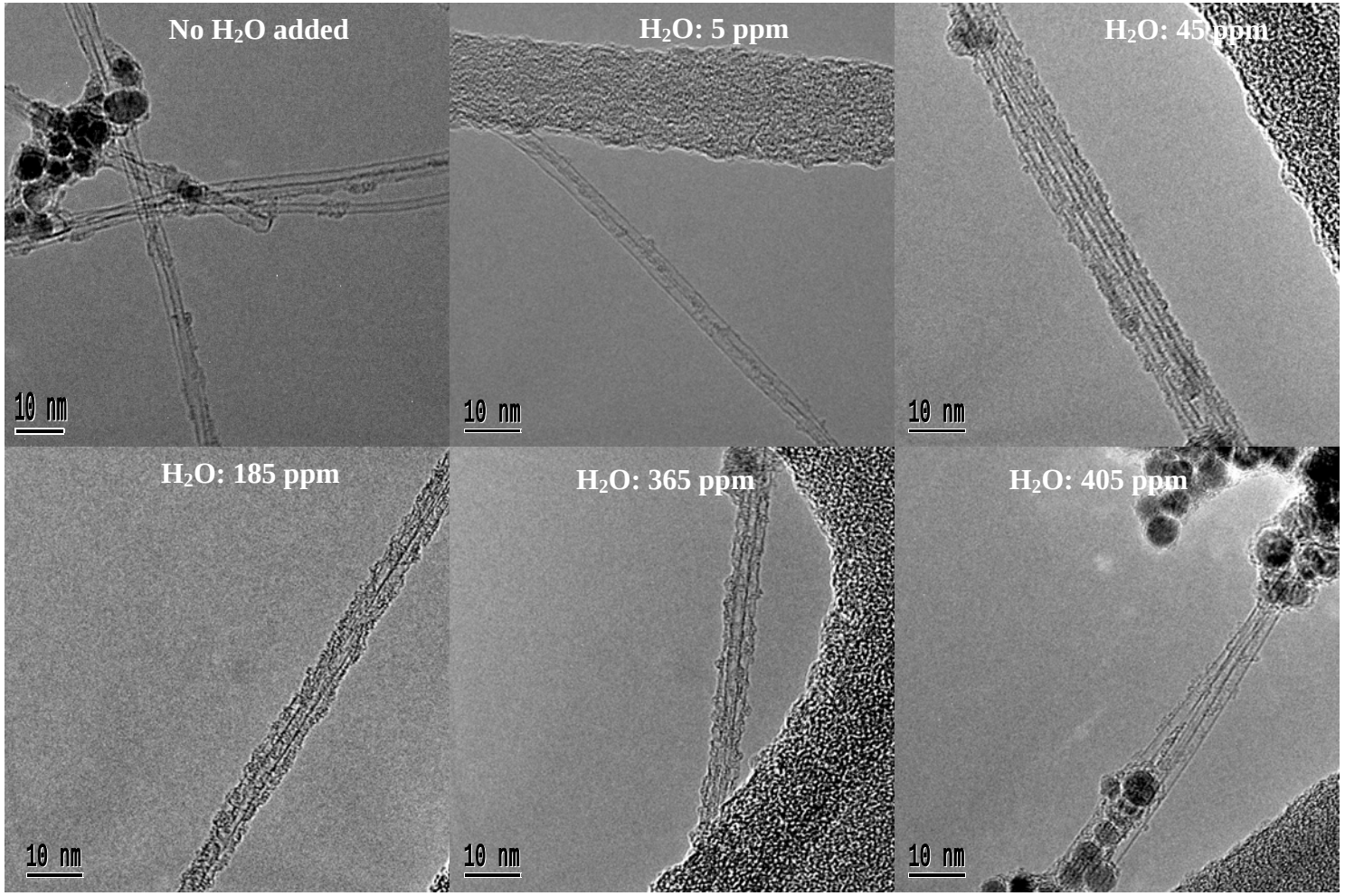

Figure S2. Effect of water vapour concentration in the ferrocene reactor at 1000 °C.

Evaporation of fullerenes

In order to determine how strongly fullerenes are attached to SWNTs, we attempted to evaporate the fullerenes from samples produced at optimal conditions. Reinke *et al.*[7] showed that fullerenes located on the graphite surface would evaporate at temperatures above 260 °C. In our experiments, the heat treatment of the samples was carried out in the temperature range of 300-700 °C in Ar/H_2 and pure He atmospheres. For this purpose, silica coated nickel or carbon coated copper TEM grids with deposited NanoBud samples were placed in a sample holder and introduced into the reactor. Heat treatments under various conditions were carried out. The samples were either introduced into a previously heated reactor (300-550 °C) or into an ambient temperature reactor which was then heated to between 340 and 700 °C (with a heating rate of 10 °C/min). The samples were then maintained in the reactor at the maximum temperatures for between 1.5 and 6 hours and subsequently cooled to room temperature inside the reactor. During the heat treatment, the total flow rate through the reactor was maintained at approximately 400 cm^3/min. A sample treated at 550 °C in Ar/H_2 atmosphere is shown in Figure S3. As can be seen from the figure, fullerenes did not tend to evaporate and, thus, were present in the sample even after the thermal treatment. The same behaviour was observed in all samples studied.

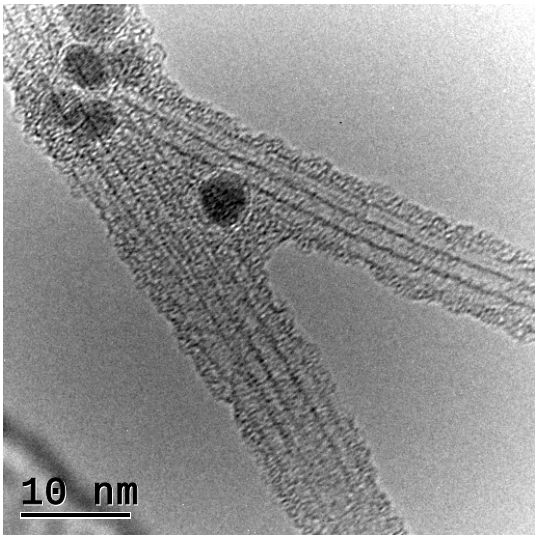

Figure S3. TEM images of NanoBuds after heat treatment at 550 °C in Ar/H_2 atmosphere.

EELS measurements

Chemical elemental analysis of the as-produced samples of NanoBuds was performed with a field emission transmission electron microscope. Typical EELS spectra at different locations of the sample are shown in Figure S4. One can observe the presence of oxygen throughout the NanoBuds.

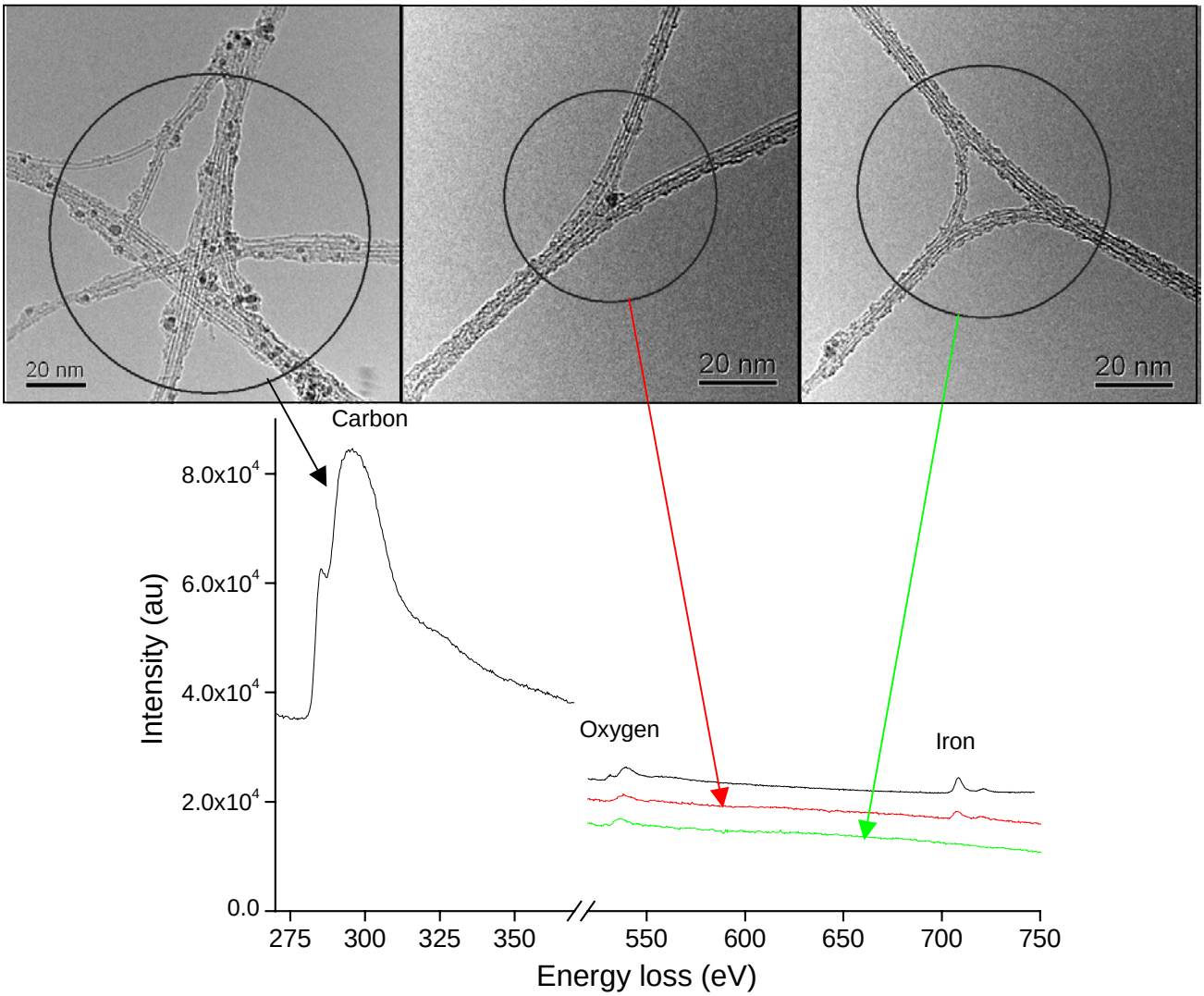

Figure S4. EELS spectra of different regions of NanoBuds.

Raman measurements

The Raman spectra measurements carried out with 633, 514 and 488 nm excitation wavelength lasers from the sample collected from the 1000 °C reactor with 100 ppm H_2O added are shown in Figure S5. The existence of a Radial Breathing Mode (RBM) and the strong G-band in the collected Raman

spectra indicated SWNT formation. A notable characteristic of the collected spectra is a weak D-band indicating a low fraction disordered carbon in the product.

As one can see from the Raman spectra, the measurements did not show any pronounced features that could be attributed to the present of fullerenes. This can be explained by the fact that strongly bound fullerenes can become highly distorted as occurs in optically polymerized fullerenes. Then even the most pronounced $A_g(2)$ pentagon pinching mode at 1469 cm^{-1} (indicative for C_{60}) completely disappears because of the low symmetry[8]. The same damping and smearing effect may also arise from the charge transfer from underlying SWNTs to fullerenes as occurs in TDAE-C_{60} due to electron-phonon coupling[7]. Another reason for the absence of the fullerene features is that different molecular weight fullerenes respond differently in Raman scattering[8,9]. Since we have a wide distribution of fullerenes in NanoBuds the amount of fullerenes of any particular mass may be insufficient for their detection by Raman spectroscopy.

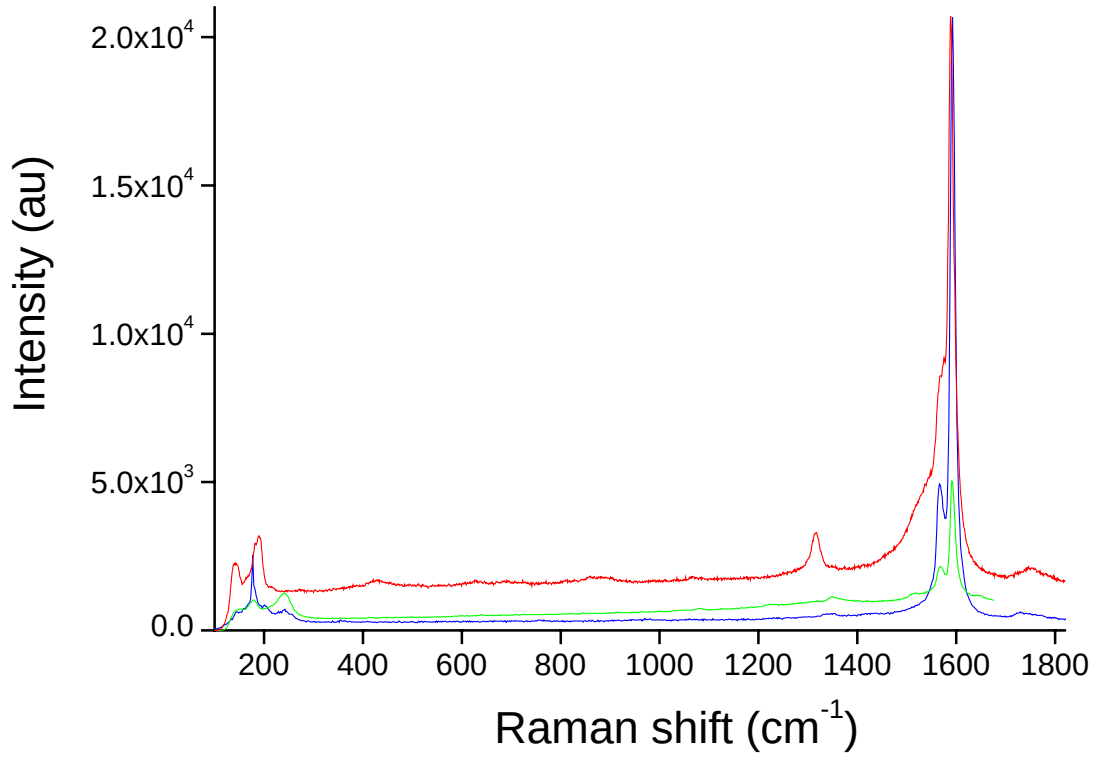

Figure S5. Raman spectra of NanoBuds carried out by using red (633 nm), green (514 nm), and blue (488 nm) lasers.

Density of states calculations

In order to better understand the STM experimental results, we calculated the density of states (DOS), which can be associated with STM I-V curves, for the studied atomic structures. For the calculations, we used the same DFT-based tight-binding model (DFTB)[10], which was used for calculating the atomic structures shown in Fig. 3.

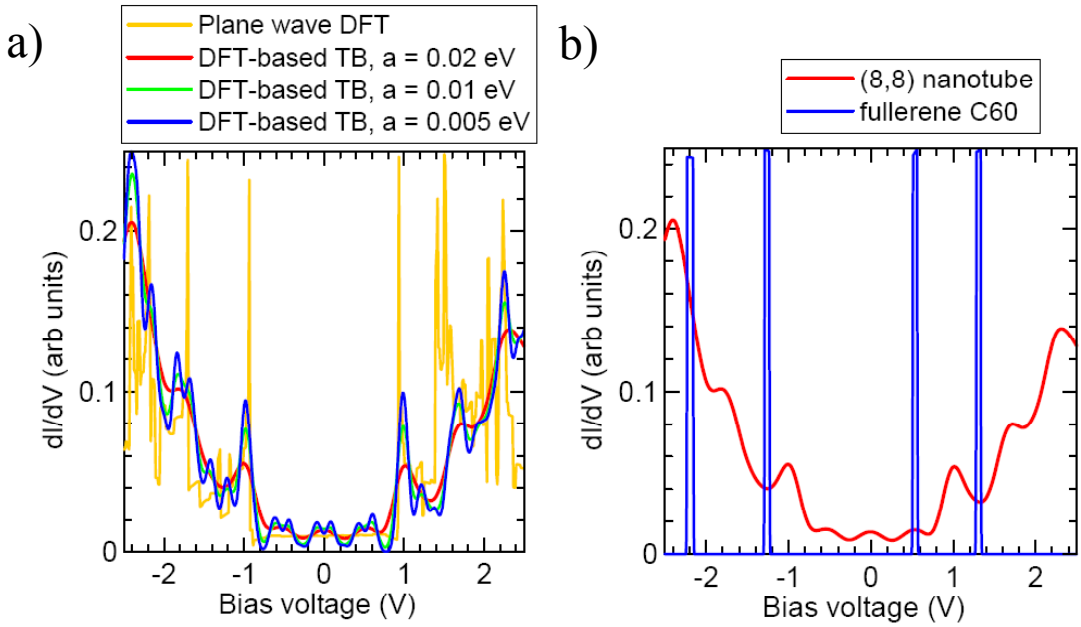

Figure S6. Comparison of DOS calculations made by DFTB and a high-accuracy plane-wave (PW) DFT models.

In order to examine the validity of the DFTB model for DOS calculations, we compared the calculated electronic structure of an ideal nanotube to that computed by a high-accuracy plane-wave (PW) DFT code VASP.[11] The PW DFT calculations were based on Projector Augmented Wave pseudopotentials[12] to describe the core electrons and the Generalized Gradient Approximation[13] for exchange and correlations. The nanotube contained 64 atoms. Its atomic structure was fully relaxed until the forces acting on atoms were less than 20 meV/A. A kinetic energy cutoff of 400 eV was found to make the total energy of the system convergent to within 1 meV. The same accuracy was also achieved with respect to the k-point sampling of the Brillouin zone (normally 9 points along the tube axis). The band structure and LDOS were calculated with a larger number of k-points (48 points). The electron density was kept fixed in these calculations. In DFTB simulations, only one (Γ) point was taken into

account. Smearing (with various values of the smearing constant *a*) was used to improve the visualization of the DOS. Figure S6a shows the DOS, which can be associated with STM I-V curves for the ideal (8,8) SWNT as calculated by the real DFT and DFTB methods. It is clear that, overall, DFTB gives the correct positions of the peaks associated with the van Hove singularities. The DOS should be constant near the Fermi energy (zero energy in all figures), but is somewhat discontinuous due to finite number of atoms in the simulation cells. Larger smearing constants smooth the solution. Figure S6b shows a discrete spectrum for an isolated fullerene C_{60}.

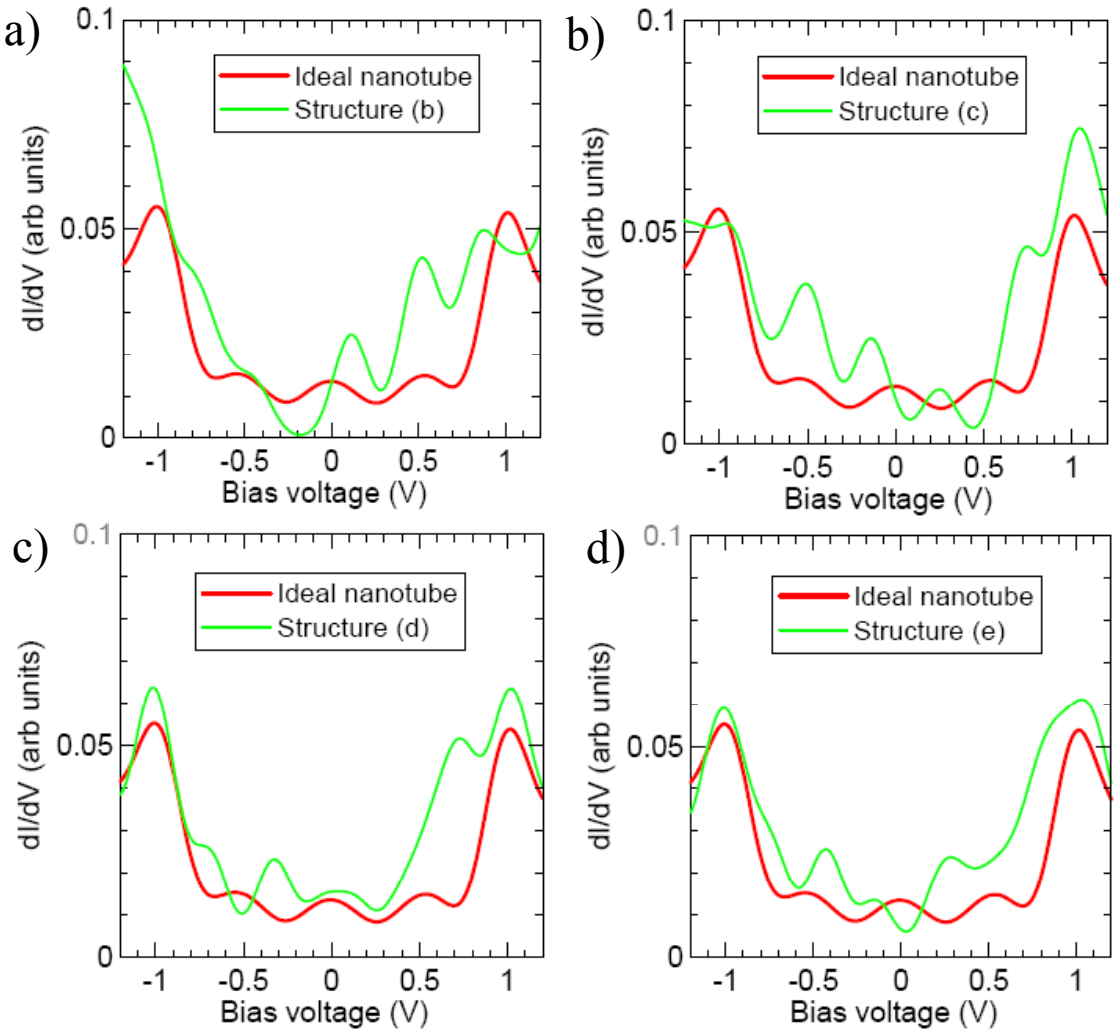

Figure S7. Comparison of DOS calculated on the basis of DFTB model for structures presented in Fig. 3b-e.

Figures S7 shows the DOS for the structures presented in Fig. 3b-e. As can be seen, the DOS calculations given in Figures S7 match well qualitatively with the STS measurement (Fig. 2e). The best correlation of the DOS calculations was found for the structure shown in Fig. 3b, where a fullerene C60

is attached to a SWNT via covalent bonds (cyclo-addition). The covalent bonding between the fullerenes and nanotubes gave rise to new states between the first van Hove singularities, as in the experiment. These states cannot be interpreted in terms of isolated (non-bonded) fullerenes, as the positions of peaks in the DOS of isolated fullerenes are different. Thus, calculations support the idea that fullerenes and SWNTs are covalently bonded, as manifested by new states near the Fermi energy.

Electron FE sample preparation and measurements

Samples for the electron FE measurements in the form of randomly oriented mats of nanotubes and NanoBuds were collected on either silver or nitrocellulose filters downstream of the ferrocene reactor. The samples were then removed from the filter, as shown in Figure S8, and placed on a gold-covered silicon wafer. A few drops of ethanol were then put on the sample to contact it to the electrode.

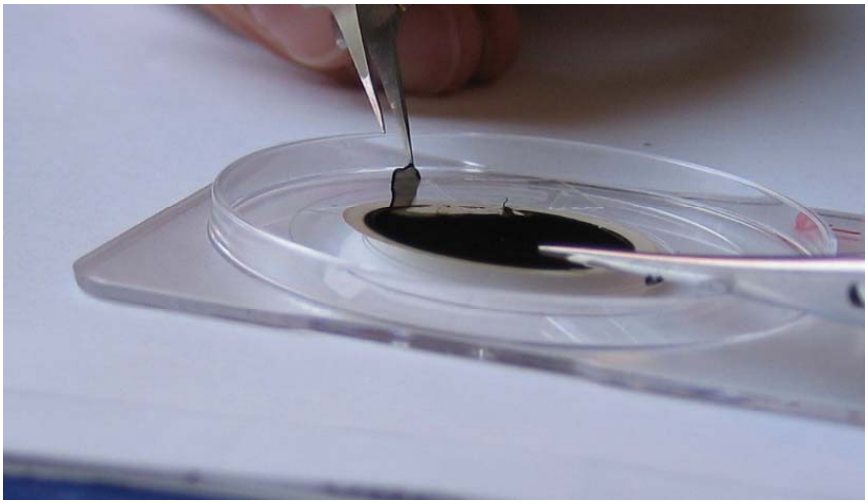

Figure S8. Photograph of NanoBud sample mat being removed from nitrocellulose filter for FE measurements.

The FE measurements were performed using a 2 mm hole and 450 μm and 675 μm spacers between the cathode and anode. The cold electron field emission measurements were carried out at a chamber pressure below $5 \cdot 10^{-7}$ Torr. A 5kV Keithley 248 Power Supply and a Keithley 6517A electrometer with pA precision were used for electric field generation and emission current monitoring, respectively.

In order to verify the stability of NanoBuds in real devices, we performed multiple voltage scans

and measured current at different field strengths for 90 min for each current (Figure S9). The long-duration measurements as well as post-experimental observation of the samples revealed no significant degradation of the NanoBud samples. The Fowler-Nordheim plot shown in Figure S10 has a characteristic knee at low currents that corresponds to the temporal current pulses seen in Figure S9. These are a manifestation of the discrete nature of the electron release from emission sites.

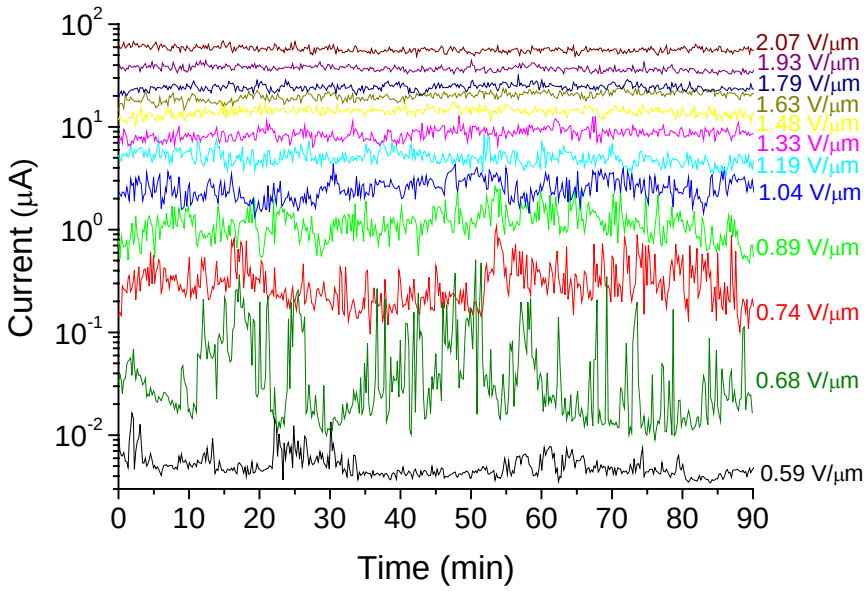

Figure S9. Temporal behaviour of the electron current at different field strengths.

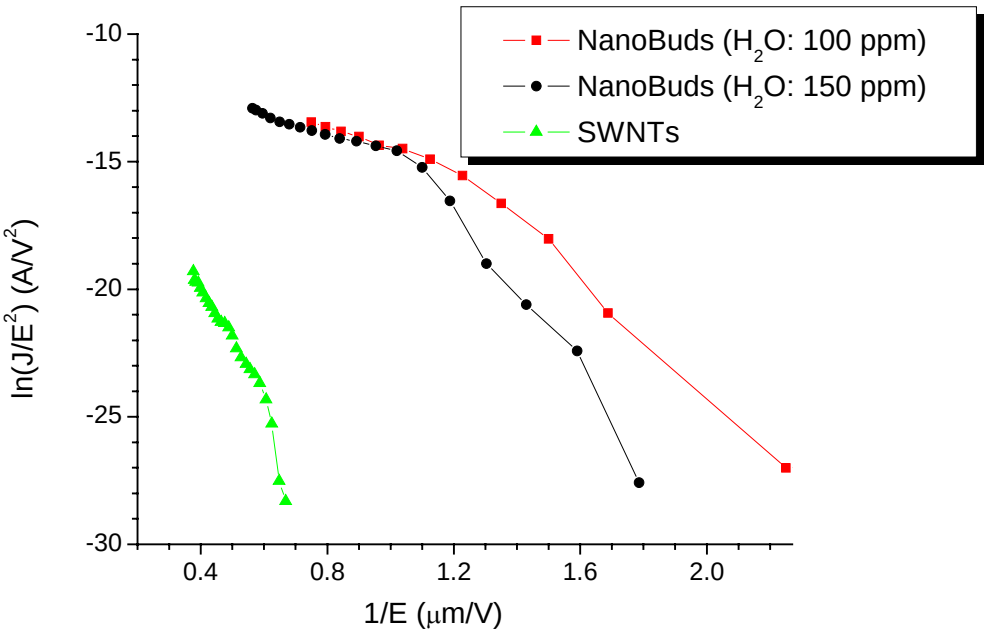

Figure S10. Fowler-Nordheim plot for the investigated samples;

The covalent nature of the bonding between SWNTs and fullerenes is supported by the threshold behaviour of electron emission from the NanoBuds, which is preserved after many hours of measurements. Our experience with carbon nanoparticles has shown that if the fullerenes were not strongly bonded to SWNTs, they would detach and create a space charge thus destroying the Fowler-Nordheim threshold dependence by transforming the latter into power law dependence.

We additionally measured the current-voltage curve in twelve voltage scans (10 scans in succession and 2 scans at a later time, all with 10 V steps) for one of the samples. As one can see from Figure S11, all curves are well grouped, scatter is within limits for fluctuations due to the discrete behaviour of the emission channels, and multiple voltage scans show no observable current degradation at the different applied voltages.

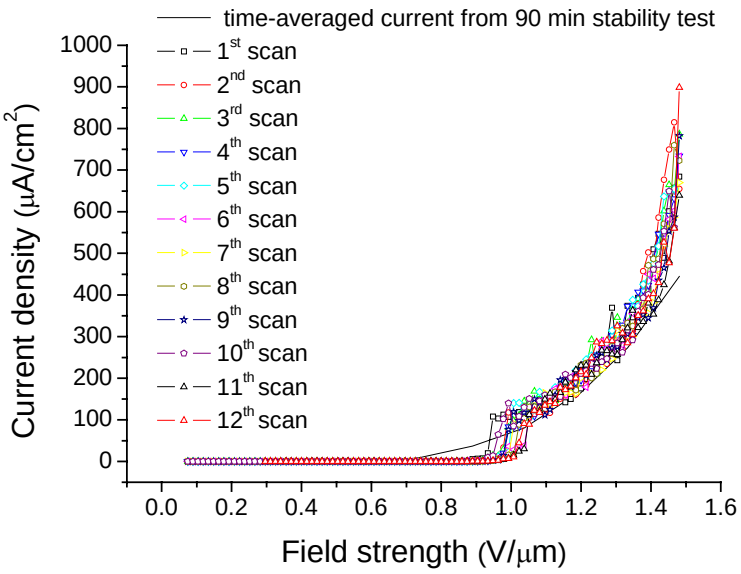

Figure S11. Multiple voltage scans. The time-averaged current (solid line) is also given.

The time-averaged current-voltage curve is also plotted in Figure S11 (the solid line; current signals for averaging were taken from Figure S9). One can see that the time-averaged current does not exactly follow the scan curves, but instead it significantly deviates at low electric fields. This occurs because, for field strengths below the knee region in the Fowler-Nordheim plot (Figure S10), the current

fluctuations are very pronounced with respect to a nearly zero background because current pulses are rare and the "instantaneous" measurement likely misses the majority of current pulse. Consequently, the current measured in a field scan is lower than the time-averaged current. The number of current pulses from single emission events per pulse duration (pulse density) increases with increasing field strength. As pulses become exponentially more frequent for higher fields approaching the knee region, they overlap and, consequently, the field scans begin to follow the time-averaged current.

It is worth noting that, using this synthesis technique, NanoBud mats for FE measurements can be prepared by direct deposition on practically any substrate at room temperature via, for instance, thermophoresis[14]. Also, since bundles of SWNTs tend to spontaneously charge in the gas phase[15], the NanoBuds can be easily deposited in patterns via, for instance, contact charging. Therefore, from an application points of view, aerosol synthesized NanoBuds may be technologically very advantageous since they can be easily deposited onto any substrate including those that are temperature sensitive and, since emission sites are present all over the tubes instead of just at the tips, they need not be aligned to the electric field.

References:

1. Moisala, A., Nasibulin, A. G., Shandakov, S. D., Jiang, H., & Kauppinen, E. I. On-line detection of single-walled carbon nanotube formation during aerosol synthesis method. *Carbon* **43**, 2066-2074 (2005).
2. Moisala, A., Nasibulin, A. G., Brown, D. P., Jiang, H., Khriachtchev, L. and Kauppinen, E. I. Single-walled carbon nanotube synthesis using ferrocene and iron pentacarbonyl in a laminar flow reactor. *Chem. Eng. Sci.* **61**, 4393-4402 (2006).
3. Nasibulin, A. G., Moisala, A., Brown, D. P., Jiang, H., & Kauppinen, E. I. A novel aerosol method for single walled carbon nanotube synthesis. *Chem. Phys. Lett.* **402**, 227-232 (2005).
4. Nasibulin, A. G., Pikhitsa, P. V., Jiang, H., & Kauppinen, E. I. Correlation between catalyst particle and single-walled carbon nanotube diameters. *Carbon* **43**, 2251-2257 (2005).

5. Nasibulin, A. G., Brown, D. P., Queipo, P., Gonzalez, D., Jiang, H., Kauppinen, E. I. An essential role of CO_2 and H_2O during single-walled CNT synthesis from carbon monoxide. *Chem. Phys. Lett.* **417**, 179-184 (2006).
6. Nasibulin, A. G. *et al.* Studies on mechanism of single-walled carbon nanotube formation. *J. Nanosci. Nanotechnol.* **6**, 1233-1246 (2006).
7. Reinke, P., Feldermann, H., and Oelhafen, C_{60} bonding to graphite and boron nitride surface. *J. Chem. Phys.* **119** 12547-12552 (2003).
8. Dresselhaus, M. S., Dresselhaus, G., and Eklund, P. C. Science of fullerenes and carbon nanotubes. Academic Press, San Diego, Boston, New York, London, Sydney, Tokyo, Toronto, 1996.
9. Kuzmany, H., June 2006, *private communication*.
10. Frauenheim, T. *et al.* Atomistic simulations of complex materials: ground state and excited state properties. *J. Phys. -Condens. Matter.* **14**, 3015-3047 (2002).
11. Kresse, G. and Furthműller, J. Efficient iterative schemes for *ab initio* total-energy calculations using a plane-wave basis set. *Phys. Rev. B* **54,** 11169 (1996).
12. Blőchl, P. E. Projector augmented-wave method. *Phys. Rev. B* **50**, 17953 (1994).
13. Perdew, J. P., Chevary, J. A., Vosko, S. H., Jackson, K. A., Pederson, M. R., Singh, D. J., Fiolhais, C. Atoms, molecules, solids, and surfaces: Applications of the generalized gradient approximation for exchange and correlation. *Phys. Rev. B* **46**, 6671 (1992).
14. Gonzalez, D. *et al.* A new thermophoretic precipitator for collection of nanometer-sized aerosol particles. *Aerosol Sci. Tech.* **39**, 801-809 (2005).
15. Gonzalez, D. *et al.* Spontaneous charging of single-walled carbon nanotubes: a novel method for the selective substrate deposition of individual tubes at ambient temperature. *Chemistry of Materials* **18**, 5052-5057 (2006).